http://eprints.gla.ac.uk/84436

Deposited on: 15 August 2013

Characterization of Fe-N nanocrystals and nitrogen bubbles in (Ga,Fe)N thin films using electron microscopy

A. Kovács,[1,a] B. Schaffer,[2,3] M. S. Moreno,[4] , J.R. Jinschek[5], A. J. Craven,[3] T. Dietl,[6,7] A. Bonanni,[8] and R. E. Dunin-Borkowski[1]

[1] Ernst Ruska-Centre for Microscopy and Spectroscopy with Electrons and Peter Grünberg Institute, Forschungszentrum Jülich, 52425 Jülich, Germany

[2] SuperSTEM, STFC Daresbury Laboratories, Keckwick Lane, Warrington WA4 4AD, United Kingdom

[3] SUPA, School of Physics and Astronomy, University of Glasgow, Glasgow G12 8QQ, United Kingdom

[4] Centro Atómico Bariloche, 8400 San Carlos de Bariloche, Argentina

[5] FEI Company, Achtseweg Noord 5, 5651 GG Eindhoven, The Netherlands

[6] Institute of Physics, Polish Academy of Sciences, al. Lotnik'ow 32/46, 02-668 Warszawa, Poland

[7] Institute of Theoretical Physics, Faculty of Physics, University of Warsaw, 00-681 Warszawa, Poland

[8] Institut für Halbleiter- und Festkörperphysik, Johannes Kepler University, Altenbergerstr. 69, 4040 Linz, Austria

[a] Author to whom correspondence should be addressed. Electronic mail: a.kovacs@fz-juelich.de

Abstract

Nanometric bubbles filled with nitrogen, located adjacent to Fe_nN ($n = 3$ or 4) nanocrystals with in (Ga,Fe)N layers, are identified and characterized using scanning transmission electron microscopy (STEM) and electron energy-loss spectroscopy (EELS). High-resolution STEM images reveal a truncation of the Fe-N nanocrystals at their boundaries with the nitrogen bubbles. A controlled electron beam hole drilling experiment is used to release nitrogen gas from a bubble *in situ* in the electron microscope. The density of nitrogen in an individual bubble is measured to be 1.4 ± 0.3 g/cm^3. These observations provide an explanation for the location of surplus nitrogen in the (Ga,Fe)N layers which is liberated by the nucleation of Fe_nN ($n> 1$) nanocrystals during the growth.

INTRODUCTION

Recent progress in nanocharacterization[1] and *ab initio* studies[2,3] has shown that the open *d*-shells of transition metal (TM) cations diluted in non-magnetic compounds not only provide localized spins but also, through charge-state-dependent hybridization with band states, contribute to the cohesive energy of the material, particularly when TM atoms also occupy neighboring sites. The resulting attractive force between the magnetic cations may lead to their aggregation, either at the growth surface during the epitaxial process, as in (Ga,Fe)N (Refs. 4-7) and for Mn cation dimers in (Ga,Mn)As,[8] or by being triggered by appropriate post-growth high-temperature annealing[9-12] or high-temperature growth,[13] as observed in (Ga,Mn)As[9-12] and (Ga,In,Mn)As,[13] respectively. Significantly, in a number of systems, the TM-rich nanocrystals that are formed in this way, such as Fe_nN ($n \geq 1$),[4-7] $MnAs$[13] or Co,[14-16] do not have a uniform distribution in the film. Instead, they tend to accumulate in planes that lie perpendicular to the growth direction, either close to the film surface[4-7,13] or at its interface with the substrate,[14-16] by a process that is referred to as nucleation-controlled aggregation.[6,16] One of the consequences of TM aggregation is that high temperature ferromagnetism in many magnetically-doped semiconductors and oxides is now assigned to the presence of such aggregates.[1,2,17] According to other schools of thought, defects[15,18] and electron-mediated interactions[19] account for robust ferromagnetism in some cases. Nanocomposite systems that contain ferromagnetic aggregates can also show enhanced magneto-optical[11] and magneto-transport properties,[20] including specific tunneling magnetoresistance.[21] A number of other functionalities are expected to be revealed in the future.[22,23]

Here, we make use of recent advances in aberration-corrected scanning transmission electron microscopy (STEM) and optimized specimen preparation techniques for electron microscopy to study, with high spatial resolution, (Ga,Fe)N layers that contain Fe_nN

nanocrystals, for which n = 3 or 4. We use annular dark-field (ADF) imaging in the STEM to record images with atomic number sensitivity (Z contrast). We show that the Fe$_n$N nanocrystals that form in the (Ga,Fe)N host are often truncated and are then associated with closely-adjacent bubbles that are filled with nitrogen. We use a combination of ADF STEM imaging and electron energy-loss spectroscopy (EELS) in an attempt to determine the nitrogen density in an individual bubble. We also release the nitrogen a bubble *in situ* in the transmission electron microscope using a focused electron beam. Our results provide new information about the location of the nitrogen that is liberated from (Ga,Fe)N during the nucleation of Fe$_n$N (n > 1) nanocrystals and have implications for the physics of (Ga,Fe)N and other nanocomposite systems, such as GaAs/MnAs and (Zn,Co)O/Co.

EXPERIMENTAL DETAILS

(Ga,Fe)N samples were grown using metal organic vapor phase epitaxy and studied in cross-sectional geometry in the TEM. The deposition process, the structure of the layers and their magnetic properties are described in detail elsewhere.[24] (Ga,Fe)N layers that were grown at 800 °C showed no evidence of secondary phases. Here, we focus on layers that were grown either at 850 °C or at higher temperatures and contain Fe-N precipitates. Specimens were prepared for TEM examination using conventional mechanical polishing and low energy (<1 keV) Ar ion milling. Great care was taken to minimize Ar ion-beam-induced artifacts. Probe-aberration-corrected STEM studies were carried out at 300 and 100 kV using FEI Titan 80-300 and Nion UltraSTEM microscopes, respectively. Electron diffraction patterns were simulated using JEMS software. An FEI Titan 80-300 environmental TEM (ETEM) microscope was used to collect EELS signals of molecular nitrogen at room temperature.

RESULTS AND DISCUSSION

A low magnification low-angle ADF (LAADF) STEM image of a (Ga,Fe)N layer that had been grown at 900 °C is shown in Fig. 1 (a). Both dislocations and Fe-N nanocrystals appear bright in the image. The dark contrast adjacent to each nanocrystal, which we observed in every (Ga,Fe)N sample that contained Fe-N nanocrystals larger than ~5 nm, is a bubble filled with nitrogen, as discussed below. The structures of the nanocrystals were determined, using nano-beam electron diffraction (NBED) (see below), to be ε-Fe$_3$N and γ-Fe$_4$N, in agreement with previous diffraction and magnetization measurements.[24] High-resolution aberration-corrected ADF STEM images of a nanocrystal and an adjacent nitrogen bubble recorded using different inner detector semi-angles are shown in Figs. 1 (b) and (c). The dissimilar crystallographic structures of the Fe-N nanocrystal and the surrounding GaN matrix result in the formation of a Moiré fringe pattern within the outline of the crystal in Fig. 1(b). The image shows that the nanocrystal is faceted, with a truncated hexagonal shape, as marked in Fig. 1(b). The volume of the missing part of the crystal is ~ 32% of the volume that it would have had if it were not truncated. By considering a nanocrystal with structure and composition of ε-Fe$_3$N and molecular nitrogen, the nitrogen content of the missing part of the nanocrystal is equivalent to the volume of a ~ 6 nm nitrogen-filled bubble at room temperature and pressure. The size of the bubble shown in Fig. 1 (b) is, however, bigger than 10 nm, suggesting that excess nitrogen may have been released during nucleation of the nanocrystal. The thin bright band of contrast that is visible around the bubble in the LAADF image may be associated with strain[25] and depends sensitively on the collection angle and sample thickness. Significant segregation of Fe, N or Ga was ruled out as an explanation for the origin of the contrast by acquiring EELS line scans across the edge of the bubble. By increasing the collection angle of the detector to acquire a high-angle ADF (HAADF) image as shown in Fig. 1(c), the contrast is

more sensitive to projected atomic number density and less to diffraction contrast. The bubble then appears with dark contrast in the recorded HAADF image.
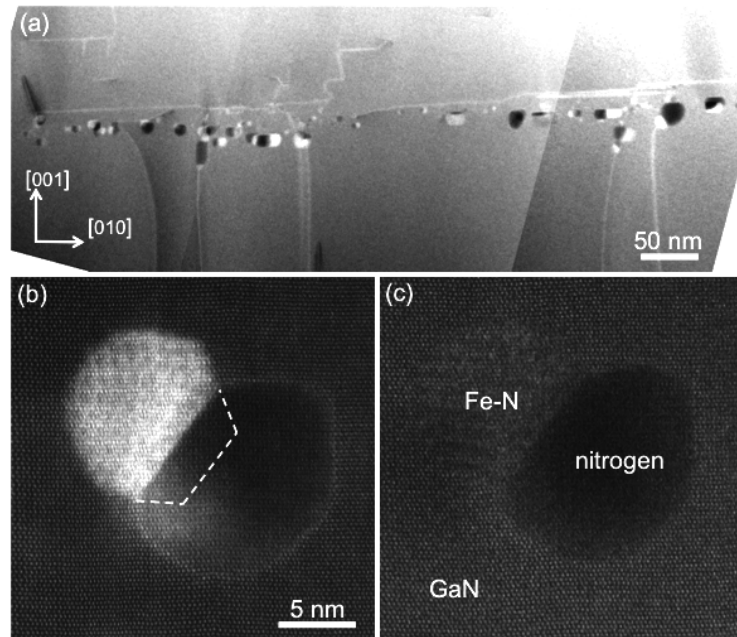

Figure 1. (a) Montage of low magnification LAADF STEM images of Fe-N nanocrystals and bubbles in a GaN layer that had been grown at 900 °C. (b) LAADF and (c) HAADF images of a 10 nm Fe-N nanocrystal and an associated nitrogen bubble. The region indicated in (b) shows an apparently truncated part of the crystal. The inner ADF detector semi-angles used were (a) 47.4, (b) 30.9, and (c) 78.4 mrad, respectively. All images were acquired at 300 kV

In each sample, Fe-N nanocrystals with a size of ~ 5 nm were also found without nitrogen bubbles adjacent to them. Figure 2 (a) shows an aberration-corrected high-resolution LAADF STEM image of a 4.5 x 3 nm Fe-N nanocrystal that had been grown at 950 °C. A Moiré fringe pattern is visible across the nanocrystal due to the overlapping Fe-N and GaN structure. The structure of a different nanocrystal from the same sample was studied using nano-beam electron diffraction as shown in Fig. 2 (b). A parallel electron beam of diameter ~ 1 nm was used to record diffraction patterns both from the Fe-N nanocrystal and from the GaN

matrix, which was used as standard for lattice parameter determination. This procedure showed that nanocrystal was ε-Fe$_3$N. Figure 2 (c) shows a simulated diffraction pattern of ε-Fe$_3$N and GaN, which provides a good qualitative match to the experimental pattern shown in Fig. 2 (b). The epitaxial relationship is inferred to be (001)[100]GaN // (001) [210]ε-Fe$_3$N. The simulated diffraction pattern was determined using lattice parameters for ε-Fe$_x$Ny obtained from Leineweber et al..[26] The lattice parameter of the ε-Fe$_3$N nanocrystal, measured along the *b* axis is 0.455±0.01 nm, which is slightly shorter than that of bulk ε-phase with composition of ε-Fe$_3$N. Such a lattice distortion can be caused either by strain or by non-stoichiometric nanocrystal composition. The results of a compositional measurement made across an ε-Fe$_3$N nanocrystal and the GaN host by collecting a linescan of N-*K* edge and Fe-*L* edge EELS spectra are shown in Figs. 2 (d) and (e). A small dip in the measured N concentration and a clear Fe peak are consistent with the presence of an Fe-rich nanocrystal.
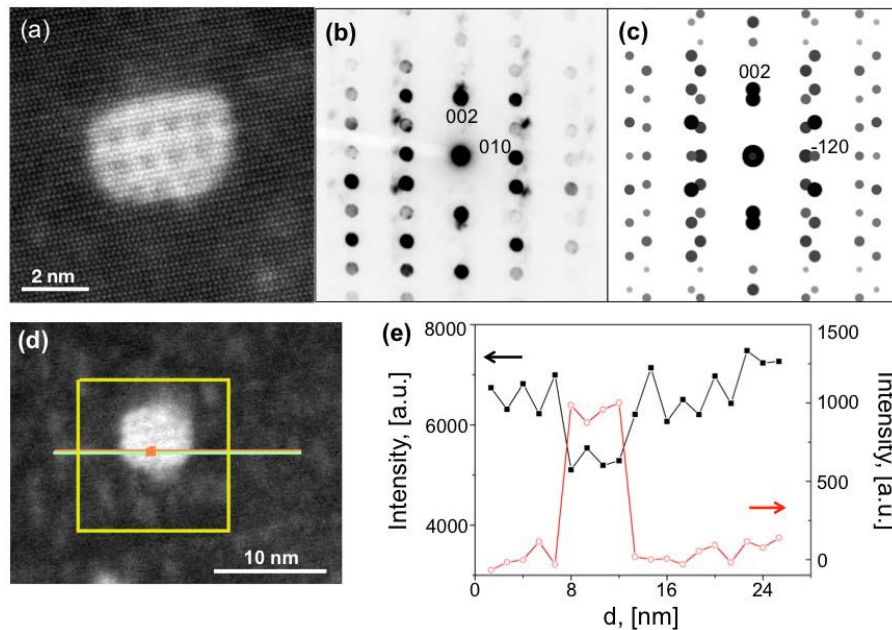

Figure 2. LAADF STEM images and diffraction patterns acquired at 300 kV from ε-Fe$_3$N nanocrystals without adjacent nitrogen bubble. (a) LAADF STEM image acquired using an inner ADF detector semi-angle of 48 mrad. (b) Experimental and (c) simulated NBED patterns

of an ε-Fe$_3$N nanocrystal in a GaN host. (d) LAADF STEM image of a different crystal, showing the region that was used for subsequent EELS analysis. The probe convergence and effective collection semi-angles were both ~ 25 mrad. (e) EELS signals corresponding to Fe (red) and N (black) recorded along the line indicated in (d).

High-resolution HAADF STEM images and diffraction patterns acquired from a γ-Fe$_4$N nanocrystal in GaN are shown in Fig. 3 for a sample that had been deposited at 950 °C. The nanocrystal had dimensions of approximately 50 x 26 nm. However, part of it is missing, where a nitrogen bubble has formed, as shown in Fig. 3 (a). The relatively large size of the nanocrystal allowed a conventional selected area electron diffraction (SAED) pattern to be recorded, containing weak reflections from the nanocrystal in addition to the reflections from GaN. Figures 3 (b) and (c) show experimental and simulated SAED patterns, from which the epitaxial relationship was inferred to be (002)[100]GaN//(-111)[110]γ-Fe$_4$N. Interestingly, a tetragonal distortion of -2.4 % was inferred in the measured lattice spacing of the γ-Fe$_4$N nanocrystal using the GaN reflections as a reference. A high-resolution HAADF STEM image of the lower interface between the γ-Fe$_4$N nanocrystal and GaN where the bright dots are Fe and Ga columns is shown in Fig. 3 (d). The structure of this interface is particularly interesting, since it is incoherent, with no dislocations observed in the γ-Fe$_4$N despite the misfit of 5.4 % between the (111)$_{Fe-N}$ and (011)$_{GaN}$ lattice plane spacing. Moreover, a spacing of of 0.34 nm is present between the γ-Fe$_4$N and GaN, as shown in Fig. 3 (e). The measured Ga-Ga peak-to-peak distance of 0.26±0.1 nm in GaN and the measured Fe-Fe distance of 0.215±0.1nm in γ-Fe$_4$N are close to the expected values of 0.259 and 0.216 nm for these structures. In the [111] direction, the γ-Fe$_4$N structure consists of modulated Fe and N layers. It is reasonable to suggest that the first layer of the γ-Fe$_4$N nanocrystal is N-rich, based on the dark contrast visible in the gap in the HAADF STEM image of the interface. The schematic model shown in

Fig. 3 (f) shows the possible interface structure. A high-resolution HAADF STEM image of the orthogonal interface between the γ-Fe$_4$N nanocrystal and the GaN host is shown in Fig. 3 (g). The misfit between the (002)$_{GaN}$ and (111)$_{Fe-N}$ planes is 16.6 %, resulting in the presence of periodic dislocations in the γ-Fe$_4$N nanocrystal as indicated in Fig. 3 (f). The dislocations formed at every 4-5 planes with a distance of 0.9 nm and 1.1 nm between them.
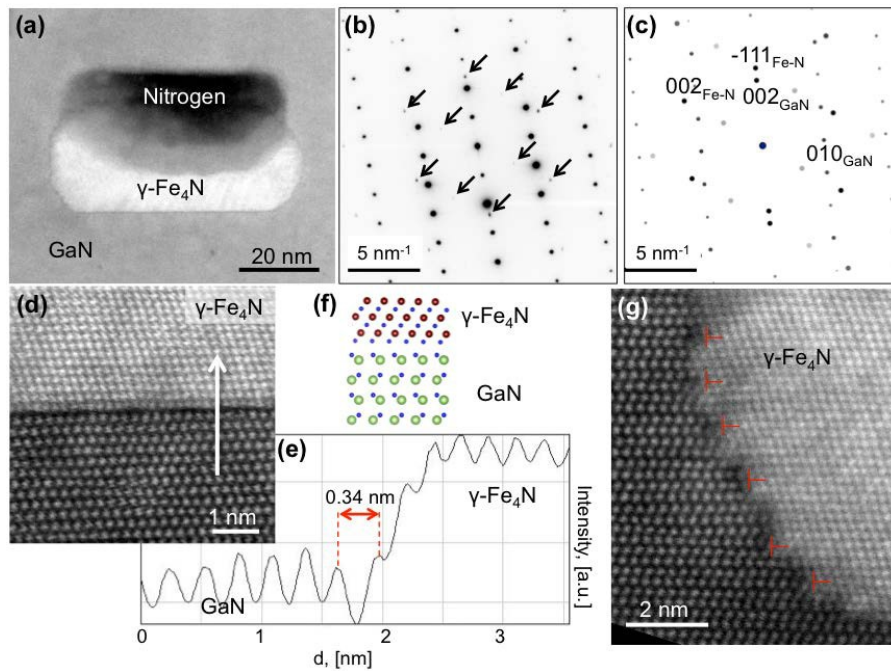

Figure 3. ADF STEM images and diffraction patterns recorded at 300 kV from a γ-Fe$_4$N nanocrystal associated with a nitrogen bubble. (a) ADF STEM image, (b) experimental and (c) simulated SAED patterns acquired from a γ-Fe$_4$N nanocrystal in GaN. (d) High-resolution aberration-corrected HAADF STEM image of the lower edge of the γ-Fe$_4$N nanocrystal shown in (a). The inner ADF detector semi-angle used for acquiring images (a), (d) and (g) was 47.4 mrad. (e) Integrated intensity scan generated along the arrow marked in (d). A spacing of ~0.34 nm is present between the last Ga row and the first Fe row. (f) Model of the interface structure inferred from the STEM image. (g) HAADF STEM image of the interface at the left side of the nanocrystal shown in (a). Misfit dislocations formed in the γ-Fe$_4$N nanocrystal are marked.

A STEM EELS measurement was performed to obtain chemical information from a single nanocrystal and an adjacent bubble embedded in the GaN host. The measurement was challenging as a result of the presence of nitrogen in each of the three phases (GaN, Fe-N and nitrogen). We studied the fine structure of the N-K edge by using a distributed dose acquisition routine (SMART[27]) in order to minimize electron beam induced damage during the experiment, which was performed at 100 kV. The convergence and collection semi-angles used were 30 and 33 mrad, respectively. An ADF STEM image and background-subtracted EELS spectra acquired from an Fe-N nanocrystal and an associated bubble in a (Ga,Fe)N layer that had been grown at 850 °C are shown in Fig. 4. The EELS line-scan spectra in Fig. 4 (b) were acquired from the area indicated by a box and an arrow shown in Fig. 4(a). Representative N-K edge spectra recorded from the GaN host, the (bubble + GaN) and the (Fe-N nanocrystal + GaN) are shown in Fig. 4 (c). The spectrum recorded from the GaN host shows a characteristic three-peaked structure between 400 and 405 eV. This feature also appears in EELS spectra collected from the Fe-N/bubble complex, as they are embedded in the GaN host. However, the first peak in the spectrum that was collected from the bubble, at 400 eV, is significantly higher than that recorded from either the Fe-N particle or the GaN alone. By normalizing the N-K edge tails, a difference in the heights of the second and third peaks of the N-K edge appears between the spectra recorded from the GaN and (GaN + bubble) regions. This difference is associated with the contribution of the bubble to the peak intensities. In order to interpret the fine structure of the N-K edge spectra, an EELS spectrum was recorded from molecular N_2 gas in an environmental TEM.[28] The N-K edge fine structure of GaN was also calculated using self-consistent real-space multiple-scattering calculations,[29] as implemented in the FEFF9.05

density functional theory code, which allows experimental parameters such as beam energy, crystal orientation and collection angle to be included. The random phase approximation was used to include core hole effects while the Hedin-Lundqvist self-energy was used to take inelastic losses into account. A characteristic single-peaked feature in the experimental spectrum recorded from nitrogen gas and multiple peaks in the spectrum simulated for GaN are visible in Fig. 4 (d). Distinct peaks in the experimental molecular nitrogen spectrum at ~ 415 eV and in the simulated GaN spectrum at ~ 423 eV can also be seen in the experimental spectra shown in Fig. 4 (c) suggesting that the spectrum recorded from the (bubble + GaN) is indeed a superposition of spectra from molecular nitrogen and GaN.
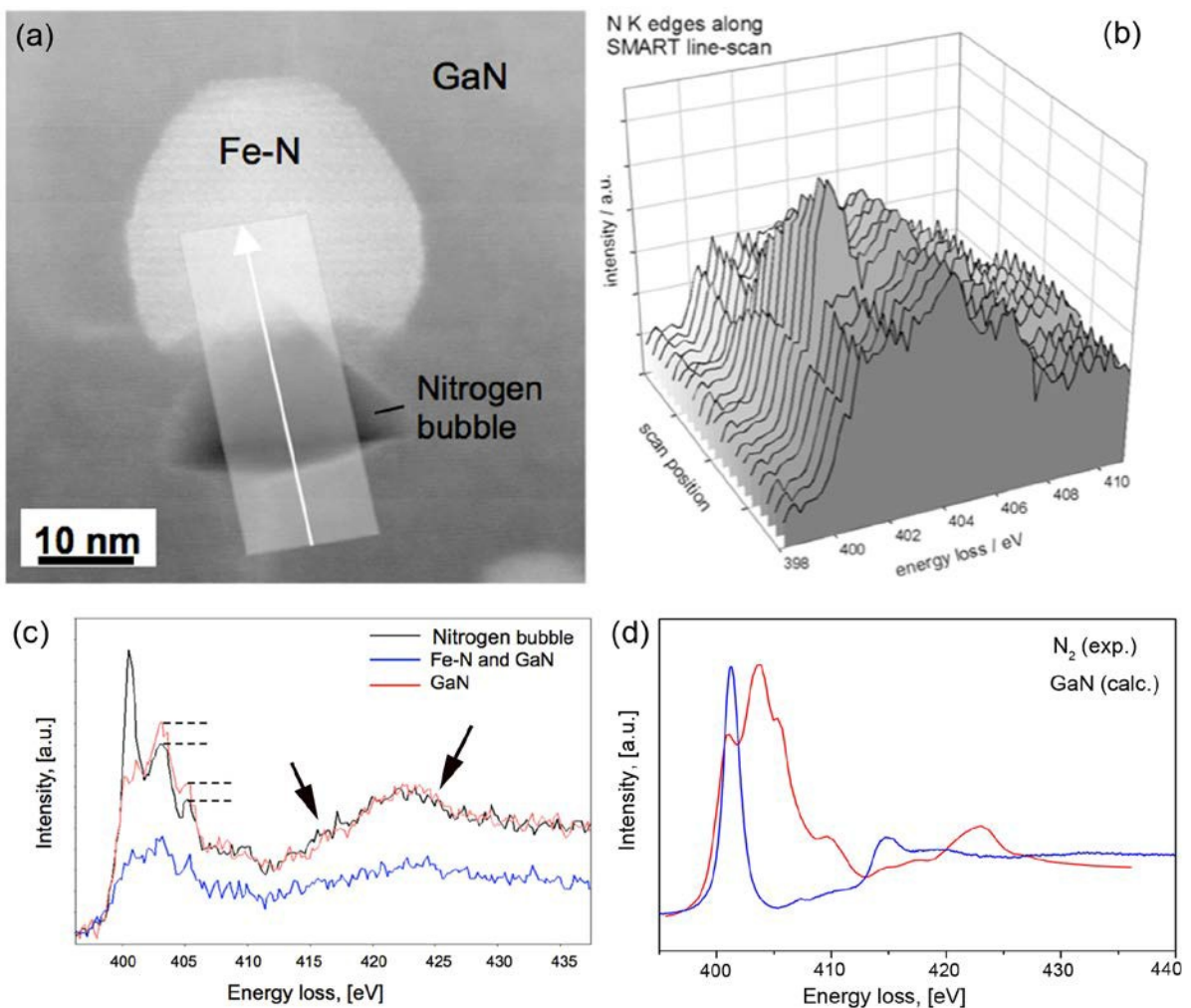
Figure 4. (a) ADF STEM image and (b) background-subtracted N-K edge EELS spectra acquired at 100 kV from a bubble, an Fe-N nanocrystal and the GaN host. The inner ADF detector semi-angle was XX mrad. The probe convergence and collection semi-angles used to acquire the EELS spectra were 30 mrad and 33 mrad, respectively. The box and arrow in (a) show the positions used for the line scan measurements. (c) Representative spectra recorded from the (bubble + GaN), (GaN + Fe-N crystal), and GaN. The dotted lines in (c) indicate an amplitude difference associated with the reduced GaN thickness at the position of the (bubble + GaN). The arrows indicate distinct peaks associated with nitrogen and GaN (see (d)). (d) Experimental EELS spectrum recorded from nitrogen gas in an ETEM at 300 kV, shown alongside a spectrum calculated for the N-K edge in GaN. The experimental spectrum was recorded at nitrogen gas pressure of 20 mbar.

Figure 5 shows the result of an experiment that provides direct evidence for the presence of nitrogen gas in the bubble adjacent to the Fe-N nanocrystal shown in Fig. 4, obtained by making use of a focused electron beam to burst it *in situ* in the electron microscope. A stationary sub-Å-diameter electron beam with a current of 350 pA was used to create a hole in the specimen at the position of the bubble, while recording an EELS spectrum every 40 s. Figures 5 (a) and (b) show ADF STEM images of the nitrogen bubble and part of the adjacent Fe-N nanocrystal recorded before and after hole formation, respectively. The bubble shape can be seen to change during the experiment. The intensity of the characteristic first peak in the N-K edge spectrum at 400 eV was observed to decrease suddenly when the nitrogen gas was released after irradiation for 600 s, as shown in Figs. 5 (c)-(e). After hole formation, the N-K edge fine structure is the same as that measured from GaN alone (see Figs. 4 (b) and (c)).
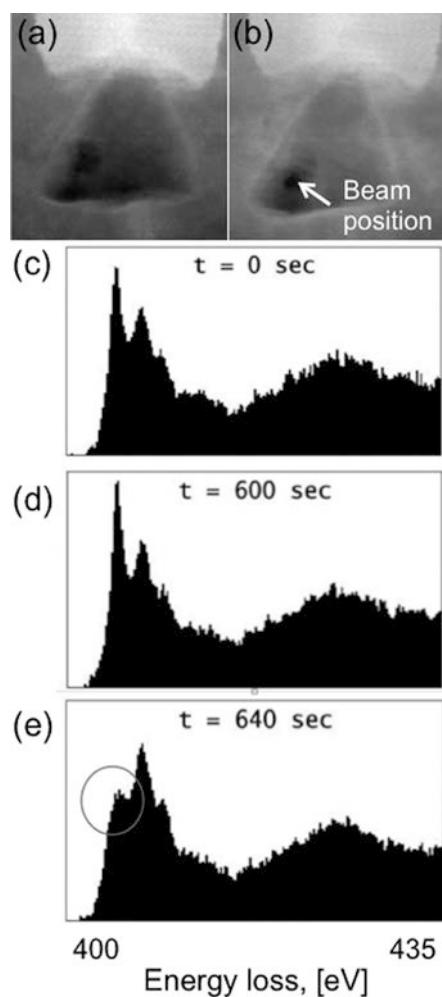
Figure 5. (a), (b) ADF STEM images of the same Fe-N nanocrystal and nitrogen bubble as in Fig. 4, recorded while drilling a hole in the specimen using a stationary 100 kV focused electron beam after at (a) 0 and (b) 640 s. (c)–(e). Background-subtracted EELS spectra taken from a time series of N-K edge measurements. After approximately 10 min. (between spectra (d) and (e)), a hole forms in the specimen and the nitrogen gas is released from the bubble. The intensity of the first peak in the spectrum is then reduced.

The study of a molecular-nitrogen filled bubble in solid GaN is very challenging using TEM and EELS. First, the radiation damage introduced to the specimen by the electron beam needs to be considered, including (i) ionization (radiolysis), (ii) sputtering by knock-on and (iii) specimen heating.[30,31] Ionization is likely to result a chemical shift of the N-K edge, but not to a

have significant effect on the overall intensity of the EELS spectrum. Knock-on damage of GaN is also unlikely, since the bulk threshold knock-on energies for N and Ga atom displacements are 32 and 24 eV, which require electron energies of 180 and 510 keV, respectively, for the production of Frenkel pair point defects.[32] With regard to the nitrogen in the bubble, the combined effect of displacement and ionization can result in weakening or splitting the atomic bonds in nitrogen dimers. The complexity of the system is even greater as a result of the presence of Fe in the vicinity of the bubble, since an Fe-based catalyst is used for splitting nitrogen bonds in the presence of hydrogen in the Haber-Bosch process.[33] With regard to specimen heating, the temperature rise[31] is expected to be $\Delta T \sim \langle E \rangle (2R_0/b) / (4\pi\kappa\lambda)$, where $\langle E \rangle$ is the mean energy loss per inelastic scattering event, R_0 is the distance from the beam position to the conductive part of the TEM stage or grid bar, b is the probe size, κ is the thermal conductivity of the specimen and λ is the inelastic mean free path. A 100 kV STEM probe is therefore expected to increase the temperature of a ~100 nm thick specimen by only a few degrees, as GaN has a thermal conductivity of $\kappa = 130$ W m^{-1}K^{-1}. However, the molecular nitrogen gas has a thermal conductivity of $\kappa = 0.026$ W m^{-1}K^{-1}, which is four orders of magnitude lower than that of GaN. Electron beam induced heating may therefore be negligible for GaN at 100 kV, but it is less well understood for nitrogen gas in GaN. Additional energy cascade processes, e.g. photoelectrons and Auger electrons, may also transfer energy to the GaN host rather than to the nitrogen gas, due to the greater mean free path of electrons in the gas than in the bubble.

The complexity of the experiment performed on the nitrogen-filled bubble in GaN is also illustrated by the dynamic transformation of the bubble shape during STEM imaging and EELS, as shown in Fig. 6. The truncated shape of the bubble is seen to transform first into a trapezoid and then to a triangular shape, thereby reducing its contact area with the Fe-N nanocrystal, as shown in Figs. 6 (a) – (d). The size of the Fe-N nanocrystal does not change

significantly. Only the interface between the nanocrystal and the bubble becomes more curved during the experiment, as marked by arrows in Figs. 6 (b) – (d).
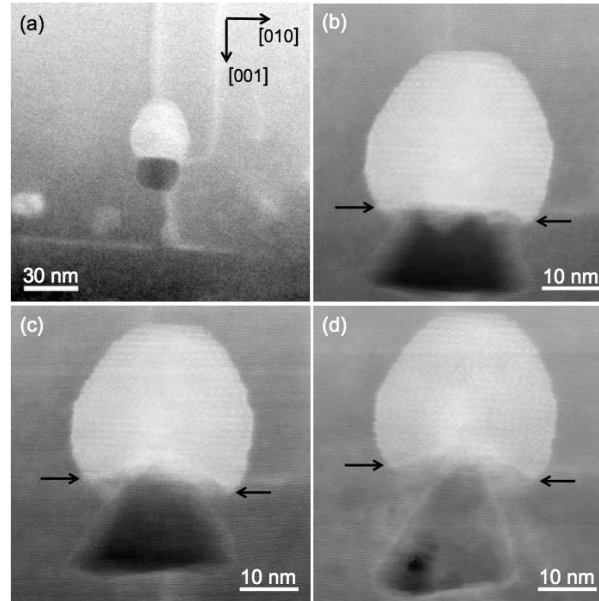

Figure 6. ADF STEM images of the same Fe-N and nitrogen bubble complex as in Figs. 4 and 5, showing shape changes undergone by the nanocrystal and the bubble during the experiments. (a) One of the first scans performed at low magnification; (b) a few scans later at medium resolution; (c) ~ 14 minutes later and (d) after the drilling experiment, ~ 120 minutes after (b). The black arrows indicate changes to the interface between the Fe-N nanocrystal and the nitrogen bubble. The experimental conditions are the same as in Fig. 4.

The nitrogen pressure in the bubble can in principle be determined from an EELS measurement by using the expression $[I_{B+GaN}/I_{GaN}] = [\rho_{N(B)} \cdot d_B + \rho_{GaN} \cdot (d_{GaN} - d_B)]/\rho_{GaN} \cdot d_{GaN}$ where I, ρ, and d are the integrated intensities of the energy-loss peaks, the nitrogen densities and the specimen thicknesses respectively of the nitrogen bubble and the GaN host. The total specimen thickness was measured to be $d_{GaN+B}=110 \pm 10$ nm from a low-loss EELS intensity measurement. There are 44 nitrogen atoms per nm^3 in GaN, which corresponds to a nitrogen

density $\rho_{N(B)}$ of 1.026 g/cm^3. The background-subtracted N-K edge peaks were integrated in the energy range between 398 and 448 eV. On the assumption of single scattering and that the bubble is spherical with a diameter d_B ~ 20 nm, the density of the nitrogen was estimated to be 1.4 ± 0.3 g/cm^3, which corresponds to a gas pressure of ~ 3 GPa at 300 K according to a N$_2$ pressure – density isotherm calculated by Strak et al.,[34] or to ~ 2.8 GPa according to a volume – pressure diagram for N$_2$ determined by Mills et al.[35] Bubbles with higher densities of (probably solid) nitrogen have been found in sapphire close to a GaN/sapphire interface by Matsubara et al.,[36] due to nitridation of the surface. Our pressure estimate is simplified, as it does not consider differences in scattering cross-section between the bubble and the GaN or the unknown temperature of the bubble resulting from the large thermal conductivity difference between nitrogen gas and the GaN host. An approach similar to that used by Walsh *et al.*[37] to measure the density and pressure of the gas in helium bubble in an irradiated Ni-Fe-Cr alloy could be used in a future study of the pressure of nitrogen-filled bubbles adjacent to Fe-N nanocrystals in GaN.

Summary

In summary, nitrogen filled bubbles adjacent to Fe$_n$N (n = 3 or 4) nanocrystals in (Ga,Fe)N have been identified and studied using aberration-corrected ADF STEM and EELS. The Fe$_n$N nanocrystals are arranged in a planar array in the GaN matrix. Typically, nanocrystals that are larger than ~ 5 nm are found to be associated with bubbles in samples deposited above 800 °C. Larger Fe$_n$N nanocrystals appear to be truncated at their boundaries with the adjacent bubbles. ADF STEM images recorded as a function of camera length suggest the presence of strain in GaN around the nitrogen-filled bubbles. The nitrogen density in a bubble formed in a sample deposited at 850 °C was estimated to be ~1.4 g/cm^3. The nitrogen

bubble showed strong shape transformations under electron beam illumination. An *in situ* hole drilling experiment was used to record N-*K* edge spectra before and after the nitrogen gas in the bubble was released.

The presence of nitrogen bubbles provides an explanation for the location of surplus nitrogen which has been liberated by the nucleation of Fe_nN (n>1) nanocrystals with during the growth of (Ga,Fe)N epilayers. As shown in reference [4], optimization of the growth parameters during the deposition of (Ga,Fe)N can be used to control the aggregation and structure of the Fe_nN precipitates and, in principle, to eliminate the bubbles.

References

1. A. Bonanni, and T. Dietl, Chem. Soc. Rev. 39, 528 (2010).

2. K. Sato, L. Bergqvist, J. Kudrnovský, P. H. Dederichs, O. Eriksson, I. Turek, B. Sanyal, G. Bouzerar, H. Katayama-Yoshida, V. A. Dinh, T. Fukushima, H. Kizaki, and R. Zeller, Rev. Mod. Phys. 82, 1633 (2010).

3. N. Gonzalez Szwacki, J. A. Majewski, and T. Dietl, Phys. Rev. B 83, 184417 (2011).

4. A. Navarro-Quezada, T. Devillers, T. Li, and A. Bonanni, Appl. Phys. Lett. 101, 081911 (2012)

5. A. Bonanni, A. Navarro-Quezada, T. Li, M. Wegscheider, Z. Matej, V. Holy, R. T. Lechner, G. Bauer, M. Rovezzi, F. D'Acapito, M. Kiecana, M. Sawicki, and T. Dietl, Phys. Rev. Lett. 101, 135502 (2008).

6   A. Navarro-Quezada, N. Gonzalez Szwacki, W. Stefanowicz, T. Li, A. Grois, T. Devillers, M. Rovezzi, R. Jakieła, B. Faina, J. A. Majewski, M. Sawicki, T. Dietl, and A. Bonanni, Phys. Rev. B 84, 155321 (2011).

7   I. A. Kowalik, A. Persson, M. A. Nino, A. Navarro-Quezada, B. Faina, A. Bonanni, T. Dietl, and D. Arvanitis, Phys. Rev. B 85, 184411 (2012).

8   M. Birowska, C. Śliwa, J. A. Majewski, and T. Dietl, Phys. Rev. Lett. (2012).

9   J. De Boeck, R. Oesterholt, A. Van Esch, H. Bender, C. Bruynseraede, C. Van Hoof, and G. Borghs, Appl. Phys. Lett. 68, 2744 (1996).

10.   M. Moreno, A. Trampert, B. Jenichen, L. Däweritz, and K. H. Ploog, J. Appl. Phys. 92, 4672 (2002).

11.   M. Yokoyama, H. Yamaguchi, T. Ogawa, and M. Tanaka, J. Appl. Phys. 97, 10D317 (2005).

12.   J. Sadowski, J. Z. Domagała, R. Mathieu, A. Kovács, T. Kasama, R. E. Dunin-Borkowski, and T. Dietl, Phys. Rev. B 84, 245306 (2011).

13.   S. Hara, M. Lampalzer, T. Torunski, K. Volz, W. Treutmann, and W. Stolz, J. Cryst. Growth 261, 330 (2004).

14.   J. H. Park, M. G. Kim, H. M. Jang, S. Ryu, and Y. M. Kim, Appl. Phys. Lett.84, 1338 (2004).

15.   R. Lardé, E. Talbot, P. Pareige, H. Bieber,G. Schmerber, S. Colis, V. Pierron-Bohnes, and A. Dinia, J. Am. Chem. Soc. 133, 1451 (2011).

16. M. Sawicki, E. Guziewicz, M. I. Łukasiewicz, O. Proselkov, I. A. Kowalik, W. Lisowski, P. Dłużewski, A. Wittlin, M. Jaworski, A. Wolska, W. Paszkowicz, R. Jakieła, B. S. Witkowski, L. Wachnicki, M. T. Klepka, F. J. Luque, D. Arvanitis, J. W. Sobczak, M. Krawczyk, A. Jablonski, W. Stefanowicz, D. Sztenkiel, M. Godlewski, and T. Dietl, arXiv:1201.5268.

17. T. Dietl, Nat. Mater. 9, 965 (2010).

18. J. M. D. Coey, K. Wongsaprom, J. Alaria, and M. Venkatesan, J. Phys. D: Appl. Phys. 41, 134012 (2008).

19. Y. Yamada, K. Ueno, T. Fukumura, H. T. Yuan, H. Shimotani, Y. Iwasa, L. Gu, S. Tsukimoto, Y. Ikuhara, and M. Kawasaki, Science 332, 1065 (2011).

20. W. Heimbrodt, P. J. Klar, S. Ye, M. Lampalzer, C. Michel, S. D. Baranovskii, P. Thomas, and W. Stolz, J. Supercond.. 18, 315 (2005).

21. R. Akiyama, S. Ohya, P. N. Hai, and M. Tanaka, J. Appl. Phys. 111, 063716 (2012).

22. H. Katayama-Yoshida, K. Sato, T. Fukushima, M. Toyoda, H. Kizaki, V. A. Dinh, and P. H. Dederichs, phys. stat. sol. (a) 204, 15 (2007).

23. T. Dietl, J. Appl. Phys. 103, 07D111 (2008).

24. A. Navarro-Quezada, W. Stefanowicz, T. Li, B. Faina, M. Rovezzi, R. T. Lechner, T. Devillers, F. d'Acapito, G. Bauer, M. Sawicki, T. Dietl, and A. Bonanni, Phys. Rev. B 81, 205206 (2010).

25. Z. Yu, D.A. Muller, and J. Silcox, J. Appl. Phys. 95, 3362 (2004).

26. A. Leineweber, H. Jacobs, F. Hüning, H. Lueken, and W. Kockelmann, J. All. Comp. 316, 21 (2001)

27. K. Sader, B. Schaffer, G. Vaughan, R. Brydson, A. Brown, and A. Bleloch, Ultramicroscopy 110, 998 (2010).

28. J. R. Jinschek and S. Helveg, Micron 43, 1156 (2012)

29.   M. S. Moreno, S. Lazar, H.W. Zandbergen and R.F. Egerton, Phys. Rev. B 73, 073308 (2006)

30.   D. B. Williams and C. B. Carter, Transmission Electron Microscopy: A Textbook for Materials Science, (Springer 2009) pp. 64-68

31.   R.F. Egerton, Ultramicroscopy 127, 100 (2012)

32.   A. Ionascut-Nedelcescu, C. Carlone, A. Houdayer, H. J. von Bardeleben, J.-L. Cantin, and S. Raymond, IEEE Trans. Nucl. Sci. 49, 2733 (2002)

33.   See, for example, M. D. Fryzuk and S.A. Johnson, Coor. Chem. Rev. 200-202, 379 (2000)

34.   P. Strak and S. Krukowski, J. Chem. Phys. 126, 194501 (2007)

35.   R. L. Mills, B. Olinger, and D. T. Cromer, J. Chem. Phys. 84, 2837 (1986)

36.   T. Matsubara, and K. Shoda, Jap. J. Appl. Phys. 45, 279 (2006)

37.   C. A. Walsh, J. Yuan, and L.M. Brown, Phil. Mag. A 80, 1507 (2000)